

# HIGH PERFORMANCE Nb<sub>3</sub>SN CAVITIES\*

D.L. Hall<sup>†</sup>, M. Liepe, R. D. Porter, T. Arias, P. Cueva,  
D. B. Liarte, D. A. Muller, J. P. Sethna, N. Sitaraman  
Cornell Laboratory for Accelerator-Based Sciences and Education (CLASSE),  
Ithaca, NY 14853, USA

## Abstract

In recent years, 1.3 GHz single-cell cavities coated with Nb<sub>3</sub>Sn at Cornell University have repeatedly demonstrated quality factors of 10<sup>10</sup> at 4.2 K and >15 MV/m. Ongoing research is currently focussed on the impact of intrinsic and extrinsic factors that limit the quality factor and quench field in these cavities. New single-cell cavities have been commissioned to enable further exploration of the coating parameter space. Experimental studies on both cavities and sample coupons have been supplemented by theoretical work done on layer growth, trapped vortex motion and flux entry. In this paper, we provide a comprehensive overview of the latest developments on Nb<sub>3</sub>Sn cavities, including work conducted in collaboration with the new NSF Center for Bright Beams, with a brief summary on work being done in the field at large.

## INTRODUCTION

Nb<sub>3</sub>Sn is demonstrating itself to be a promising next-generation alternative to niobium for use in SRF cavities, outperforming the best niobium cavities at 4.2 K and 16 MV/m [1–3]. However, questions still remain on how to ensure high efficiency at high gradients.

## COATING PROCEDURE

To date the best-performing Nb<sub>3</sub>Sn cavities have been fabricated using the vapour diffusion process [4], in which a niobium substrate is exposed to tin vapour in an ultra-high vacuum (UHV) furnace at temperatures above 950°C. A diagram of the custom-built UHV furnace used for coating 1.3 GHz single-cell ILC cavities at Cornell University is shown in Fig. 1. The furnace consists of a niobium chamber inserted into the main furnace hotzone, at the base of which is a small alcove in which the tin source is placed. Surrounding this alcove is a secondary heater that allows the tin source to be held at a temperature higher than that of the cavity.

The coating process is described in detail in Ref. [5], but is briefly summarised here. High purity tin, in a tungsten crucible, is placed into the alcove at the base of the furnace. Just above it, a tungsten crucible containing the nucleation agent SnCl<sub>2</sub> is placed. The niobium substrate – cavity or coupon – to be coated is lowered into the furnace, and the furnace is sealed. After a 24-48 hour degas cycle at 180°C, the chamber and source together area taken to 500°C and held

there for 5 hours to allow the nucleation agent to pre-seed the niobium substrate with tin. Following this, a temperature difference of 150°C is established between the tin source and the coating chamber. Together, they are raised to a temperature of approximately 1120°C in the chamber and 1250°C at the source. This stage, referred to as the *coating* stage, is held for the amount of time prescribed by the recipe. Often, the source heater is then turned off, and allowed to equilibrate to the temperature of the cavity, substantially reducing the rate of tin arriving at the surface. Following this *annealing* stage, the power to the furnace is cut and the entire structure is allowed to cool by radiation until 25°C, at which point the furnace is opened.

This coating process differs from that used at other labs, both historically and currently. Coating furnaces have been used at Siemens AG, the University of Wuppertal, Jefferson Lab and Fermi National Laboratory. A diagram demonstrating the differences between the different designs of coating furnace is shown in Fig. 2.

## UNIFORMITY OF THE COATED LAYER

In the first coatings at Cornell there was significant difficulty with non-uniform coatings of a single-cell cavity, which led to poor performance and significant *Q*-slope. This was resolved by introducing a temperature gradient between the source and the chamber at the beginning of the ramp up to coating temperatures, which has contributed to the exceptional performance seen in these cavities.

In particular, the first cavity coated at Cornell, denoted ERL1-5, was found to exhibit significant heating on the half-

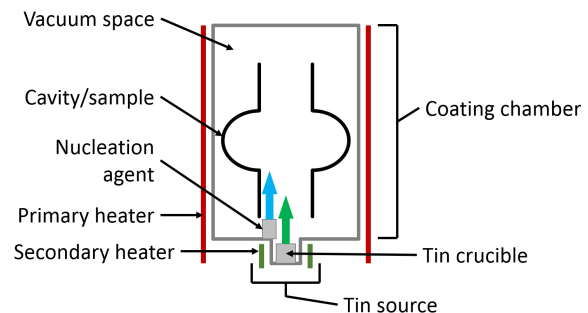


Figure 1: A simplified diagram of the Cornell UHV coating furnace. The cavity is located in a chamber placed inside the main hotzone. At the base of the chamber is the tin source, which is surrounded by a secondary hotzone that allows the source to be held at a temperature higher than that of the cavity.

\* This work was primarily supported by U.S. DOE award DE-SC0008431. This work was supported in part by the U.S. National Science Foundation under Award PHY-1549132, the Center for Bright Beams.

<sup>†</sup> dlh269@cornell.edu

Content from this work may be used under the terms of the CC BY 3.0 licence (© 2017). Any distribution of this work must maintain attribution to the author(s), title of the work, publisher, and DOI.

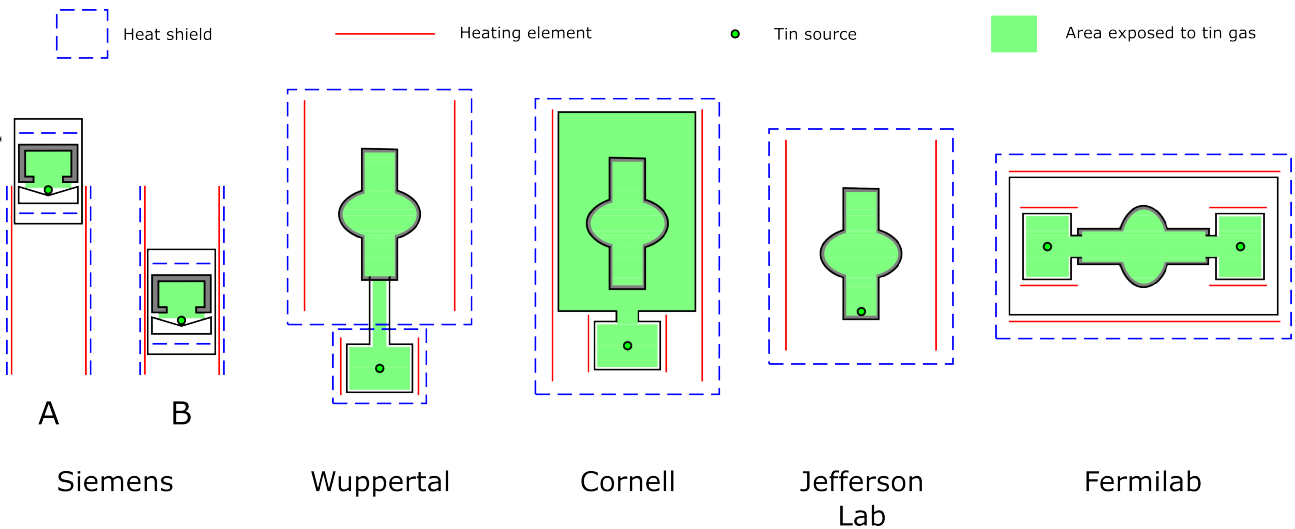


Figure 2: Simplified diagrams demonstrating the different furnace designs used to coat niobium with Nb<sub>3</sub>Sn, indicating the locations of the tin sources, hotzones, heat shields, and regions of the furnace that are exposed to the tin vapour.

cell that faced away from the source during coating. Later studies on cut-outs of this cavity [6] demonstrated that this heating was due to regions of the surface where the Nb<sub>3</sub>Sn layer is too thin to effectively screen the niobium bulk from the RF field. In addition to this, the interface between the Nb<sub>3</sub>Sn layer and the niobium bulk has often been found to be tin-depleted, as can be seen in Fig. 3. Since the transition temperature of Nb<sub>3</sub>Sn is strongly a function of the atomic-% tin content [7], this will lead to significant thermal feedback and result in the heating seen in cavities such as ERL1-5.

These regions of thin coating are seen to possess a flat surface many 10s of microns wide, and are devoid of grain boundaries when compared to nearby polycrystalline regions that are sufficiently thick. It has long been suspected that the method of diffusion of tin from the vapour into the growing layer towards the niobium interface is via already existing grain boundaries. Recent simulations performed using the joint density functional theory simulation code JDFTx [8–10] confirm that this is the case, as the mechanism for transporting tin through the bulk via niobium vacancies is slow (less than 100 nm/hr at 1400 K) when compared to tin transport through the grain boundaries. However, the latter transport mechanism is quickly suppressed by a low density of grain boundaries. These regions are therefore thinner because the absence of grain boundaries has them relying on a slower growth mechanism to grow the layer, which after 3 hours of coating is only approximately 200 nm thick or less. This can be seen in cross-sections of the Nb<sub>3</sub>Sn layer, going from the polycrystalline thick regions to the thin regions, such as in the TEM image shown in Fig. 3.

Growing the oxide layer of the substrate by pre-anodisation has been found to suppress the formation of these thin film regions [11]. Even in large grain samples of niobium, which have been found to be particularly susceptible to the formation of thin film regions, growing the niobium oxide layer to a thickness of approximately 70 nm

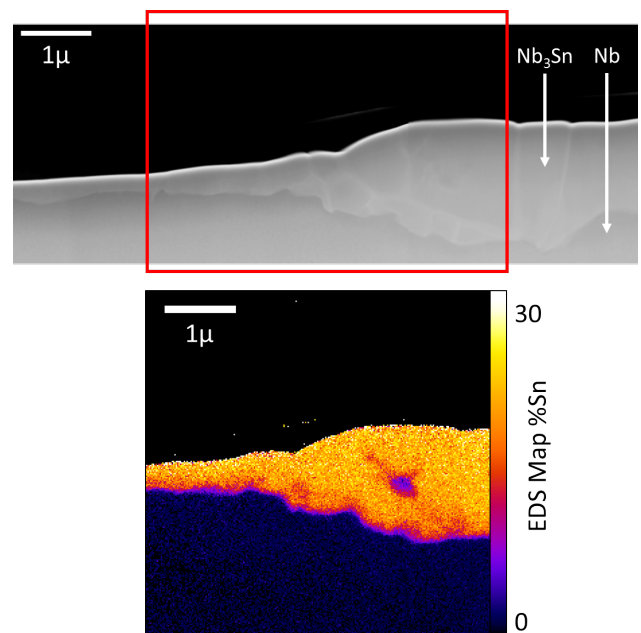


Figure 3: A cross-section of the Nb<sub>3</sub>Sn viewed in the transmission electron microscope. The upper image shows a log-mag STEM image of the Nb<sub>3</sub>Sn layer as it transitions from a thick, polycrystalline layer to a single-crystal thin layer. The lower image is an EDS map of the atomic-% tin content, showing tin depletion at the interface and also at a region inside a grain.

before coating suppressed their formation to below a detectable level of less than 1% area coverage. Indeed, even in well-performing non-pre-anodised cavities where the presence of these regions is expected to be very small, gains in performance have been demonstrated by pre-anodising the cavity before coating.

## STOP-MOTION COATING STUDY

In order to understand the mechanism by which these regions form, and why pre-anodisation is so effective in suppressing them, a special series of coating runs was performed. A number of pairs of niobium samples, fine grain of  $RRR \approx 300$ , were prepared for coating. Half of these were pre-anodised to a voltage of 30 V, corresponding to an oxide thickness of  $\approx 70$  nm. Following the standard coating recipe, pairs of samples were coated (one pre-anodised, the other not), but halting the coating process at different stages. The different stop points are shown in Fig. 4, and correspond to A) at the end of the nucleation stage at  $500^\circ\text{C}$ , B) upon reaching  $800^\circ\text{C}$  in the chamber, C) upon reaching  $950^\circ\text{C}$  in the chamber, D) upon achieving the coating temperature of  $1120^\circ\text{C}$  in the chamber, E) upon the completion of the coating step, and F) upon completion of the annealing step. Uncoated samples of niobium were also kept for reference. Each time, the cavities were hung by niobium wire in the furnace chamber at approximately the level of the equator of the cavity.

The samples were imaged in the scanning electron microscope with chemical analysis done using energy dispersive X-ray spectroscopy (EDS). This was done on a Zeiss Leo 1550 equipped with a Bruker X-Flash 6/60 EDS detector. The thin film regions can be imaged by performing an EDS map at a beam energy of 30 kV, where the penetration depth of the X-ray scan is deeper than the thickness of the thin film regions. This results in an excess of the niobium signal, which when plotted as a ratio of the tin to niobium signal can reveal the presence of the thin film regions on the surface. This is shown, as the difference between a coated layer on a naturally oxidised substrate and a pre-anodised one, in Fig. 5. To more easily compare different samples, such maps can be broken into their individual pixels, with each pixel representing a ratio  $\text{Sn}/(\text{Nb}+\text{Sn})$ . A histogram of these ratios can then be plotted, such as in Fig. 6. A Gaussian

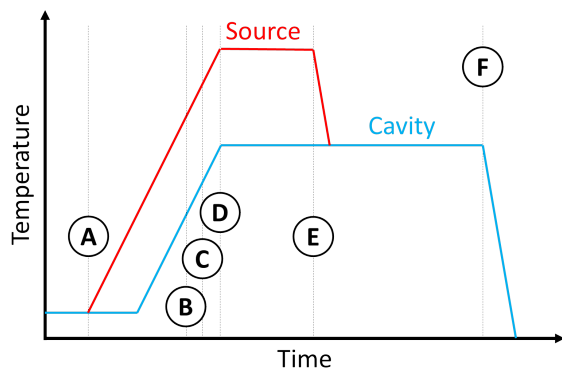


Figure 4: A schematic of the coating recipe used for the stop-motion coating series. The coating was stopped at A) the end of the nucleation stage; B) upon achieving  $800^\circ\text{C}$ ; C) upon achieving  $950^\circ\text{C}$ ; D) upon reaching the coating temperature of  $1120^\circ\text{C}$ ; E) at the end of the coating stage; and F) at the end of the annealing stage.

shape indicates a uniform coating; the presence of thin film regions is seen as a tail on the left side of the Gaussian peak. The measurement demonstrates that at all stages in the coating, the pre-anodised sample appears to be both more uniform in its coating and more developed (i.e. thicker) for any given point during the ramp up to coating temperature. The lack of a tail on the left side of the Gaussian peak for the pre-anodised sample indicates that the handover from the nucleation to the coating stage has been successful and no thin-film regions have formed.

The presence of a tail on the right side of the gaussian peak has already become evident in non-anodised samples taken up to  $950^\circ\text{C}$  (stage C in Fig. 4, indicating that non-uniform thin film regions have already begun to form. This is confirmed by SEM images of the sample coupons, shown in Fig. 7, in which non-anodised samples taken from stage C show flat regions devoid of grain boundaries. Some of these regions develop into the large, flat regions largely devoid of grain boundaries (corresponding to regions of thin film), like the one seen in stage D for the non-anodised sample. This region has already formed by the beginning of the coating stage, and is not cured by the coating process proper. This demonstrates the importance of ensuring a successful handover from the nucleation stage to the coating such that a uniform coating is guaranteed.

At any single stage, the pre-anodised substrate shows a more developed layer than its non-anodised counterpart. Observing the nucleation stages, the nucleation sites on a pre-anodised sample appear larger and closer together than for a non-anodised sample. Interestingly, the oxide layer appeared to have survived the bake at  $500^\circ\text{C}$ , with the sample still being a dark brown colour, corresponding to an oxide thickness of  $\approx 30$  nm. This difference persists when going to  $800^\circ\text{C}$ , when the tin vapour pressure has become significant. In the non-anodised sample, small crystals (assumed to be tin from the vapour) have formed on the surface; in contrast, the tin deposition in the pre-anodised sample is significantly higher. These features can be seen in the SEM images shown in Fig. 7. EDS spectra of the post-nucleation samples and the samples stopped at  $800^\circ\text{C}$  confirm that the pre-anodised

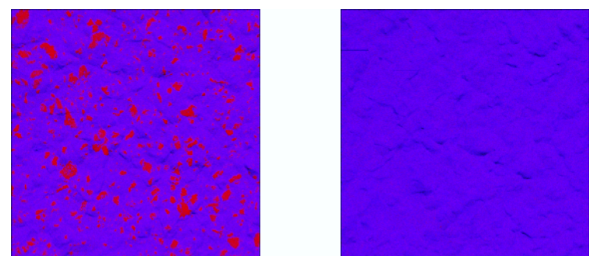


Figure 5: EDS maps of the  $\text{Nb}_3\text{Sn}$  coating of a non anodised (left) and pre-anodised (right) fine grain niobium substrate. The width of each image is 500 microns. Regions in red are areas where the  $\text{Nb}_3\text{Sn}$  layer is not thick enough to screen the substrate from the RF field. Pre-anodising the substrate before coating suppresses the formation of these regions.

Content from this work may be used under the terms of the CC BY 3.0 licence (© 2017). Any distribution of this work must maintain attribution to the author(s), title of the work, publisher, and DOI.

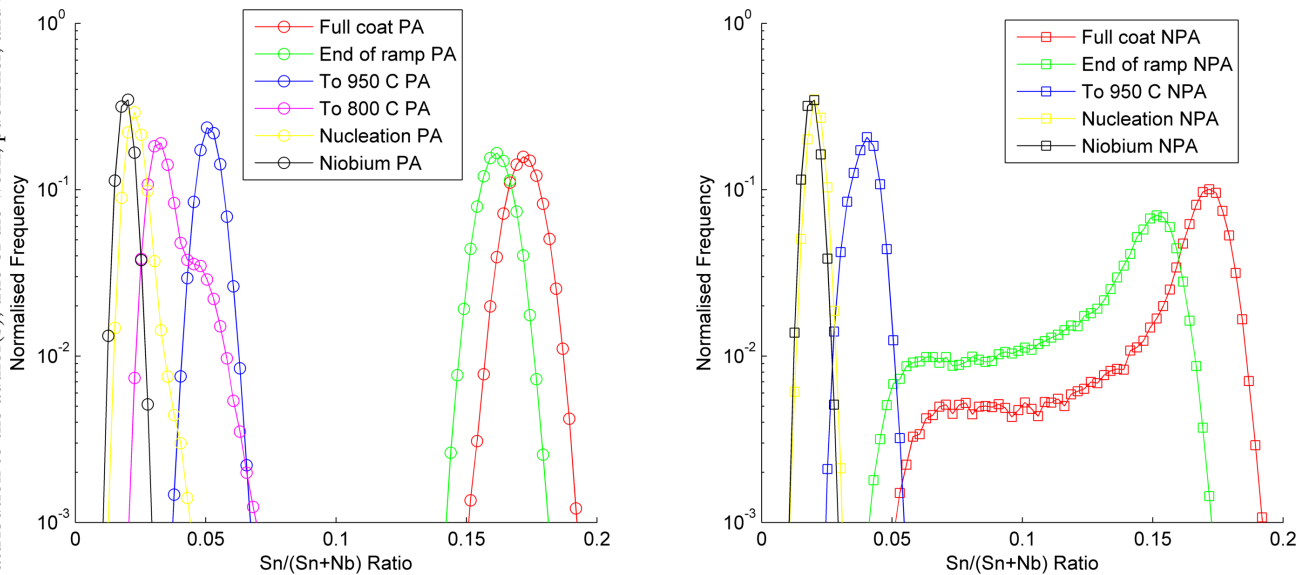


Figure 6: Histograms of the EDS maps from different samples, tallying the number of pixels for different values the ratio of the signal of tin to niobium,  $\text{Sn}/(\text{Sn}+\text{Nb})$  – on the left, for a pre-anodised sample, and the right for a sample that was not anodised before coating. A uniform distribution is indicated by a symmetrical gaussian peak. The presence of thin film regions is revealed by a tail on the left side of the peak.

samples are possessed of more tin on the surface than their counterparts.

Alongside these samples hung at the equator level, samples were coated while being placed very close to the tin source. A fine-grain niobium sample from the same sheet used to create the samples mentioned above was coated, with only its natural oxide layer, and EDS mapping revealed the presence of no thin film regions – counter to the same sample coated at the equator level in the cavity. However, a sample of large grain niobium, coated in the same position and with only the natural oxide layer, showed a significant coverage of thin film regions when coated with the same recipe. However, after stripping and pre-anodising the large grain sample, and re-coating in the same position with the same recipe, the thin film regions were found to have been suppressed.

The conclusion from this study appears to be that the survival of the nucleation sites to the point where the tin vapour can begin to sustain the growth process is critical for the surface uniformity. If the nucleation sites are absorbed into the bulk too early, or can evaporate from the surface, the few grain boundaries created will anneal and disappear, transitioning to the bulk diffusion process where the layer grows comparatively slowly. This survival is enhanced by the pre-anodisation process as the nucleation sites that are created are larger (likely due to a chemical or catalytic reaction) and can persist until the handover to the tin vapour. A similar effect is created by placing the sample close to the source, where the tin vapour pressure is higher and the handover occurs sooner. The poor coverage seen in the large grain sample is likely due to the natural oxide layer on large grain niobium being thinner than that of fine grain niobium, further stunting the size of the nucleation sites. Therefore, when coating

small, fine-grain structures such as 1.3 or 6 GHz single-cell cavities, a large temperature gradient during ramp-up to coating temperatures can ensure a successful handover. However, when coating larger structures, such as multi-cells, low-frequency structures, or samples hanging inside a large coating chamber, the tin vapour pressure during ramp-up is far lower when further from the source, and pre-anodisation is necessary to ensure the survival of the nucleation sites and a uniform coating. Although pre-anodisation will result in a lowering of the substrate RRR, and with it, the thermal conductivity, thermal simulations [12] reveal that the impact is minimal down to a RRR of even 40 when operating at 4.2 K. This is large part due to the thermal conductivity of niobium being considerably better at 4.2 K, even in spite of a lower RRR.

## CAVITY PERFORMANCE

Multiple single-cell 1.3 GHz cavities coated at Cornell have achieved  $Q_s$  of around or above  $10^{10}$  at 4.2 K and 16 MV/m, as can be seen in Fig. 8. Armed now with a better understanding of the coating process, we can propose a reason for why cavities at the University of Wuppertal or Jefferson Lab suffer from  $Q$ -slope in a manner not seen in Cornell's cavities. In the absence of a secondary heater, such as in the furnace design used at Jefferson Lab, the tin vapour pressure during the ramp up to coating temperature may be insufficient to ensure a successful handover on a non-anodised cavity. Similarly, although the furnace design at the University of Wuppertal was equipped with a secondary hot-zone around the tin crucible, and the source was held at a higher temperature than the chamber during ramp-up, the designs of the furnace [13] show a long tube between

the source and the cavity that passes between the two heat shields. It is very likely that this tube had a cooling effect on the tin vapour, essentially negating the advantage of the temperature gradient during the ramp up. The presence of thin film regions in the Wuppertal cavities, where the RF field can penetrate to the niobium substrate, is corroborated by measurements of the  $Q$  as a function of temperature in their 1 GHz cavities, which showed a sudden drop in the surface resistance at the niobium transition temperature of 9.2 K [13]. In comparison, the Siemens cavities, although not making use of a secondary heater for the tin source, benefited from the use of both pre-anodisation and nucleation agent simultaneously, while also being performed in a much smaller structure – a 10 GHz cavity – where the tin vapour pressure would be quite high even at lower temperatures.

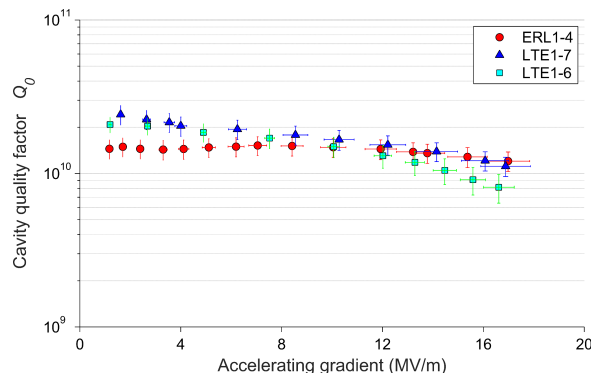


Figure 8: Performance of 1.3 GHz single-cell ILC-style cavities coated at Cornell University and operating at a bath temperature of 4.2 K.

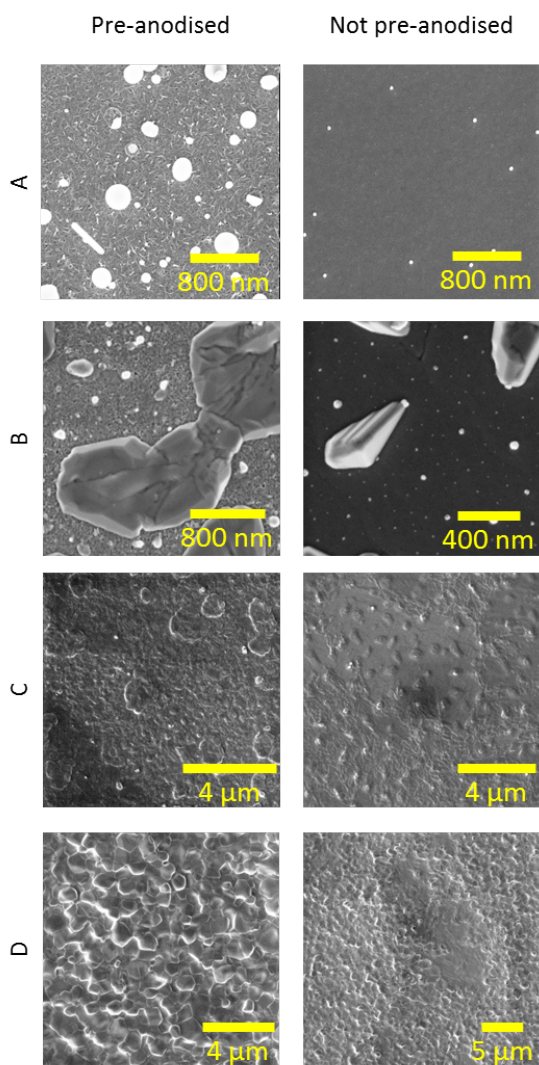


Figure 7: SEM images of the sample coupons, taken from different stages in the stop-motion coating. The left column correspond to pre-anodised samples, the right side were not anodised before coating. The letters indicate to which stage in Fig. 4 the images were taken.

Even in the absence of the  $Q$ -slope generated by thin film regions, cavities coated at Cornell still demonstrate modest  $Q$ -slope of a different nature to that seen previously. This  $Q$ -slope has been found to be attributed to losses from trapped magnetic flux that is a linear function of the applied RF magnetic field [14]. In order to ensure that the benefit of the uniform coating can be enjoyed at usable gradients above 10 MV/m, it is necessary to ensure minimal flux trapping. Due to the bi-metallic interface between the niobium and the  $Nb_3Sn$  generating thermal currents during cooldown in the presence of thermal gradients, this requires a transition through 18 K in which both thermal gradients and ambient magnetic fields are suppressed. The performance at 4.2 K for a cavity that was cooled in a thermal gradient of 200 mK/m and an ambient field of 5 mG is given in Fig. 9, and, given the functional form of the losses from trapped flux, extrapolated to an idealised cool-down in which the thermal gradients are 100 mK/m and the ambient magnetic field is 1 mG. Such a cool-down would result in a  $Q$  of  $2 \times 10^{10}$  at 16 MV/m and 4.2 K, far out-performing the best performing niobium cavities.

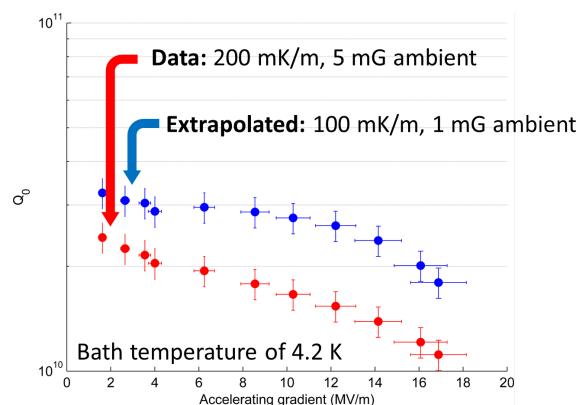


Figure 9: Performance of 1.3 GHz single-cell ILC-style cavity in the Cornell vertical test cryostat, and the same performance extrapolated to an idealised cool-down given the functional form of the losses from trapped flux.

Cavity performance is still limited to quench fields of approximately 14-18 MV/m, largely independent of coating recipe. Although higher fields have been achieved in high power pulsed testing [15], temperature mapping of a cavity operating near the quench field has revealed evidence for early magnetic flux entry at a defect [16]. The behaviour is similar to that expected for vortex entry at grain boundaries acting as Josephson junctions [17], although a thorough comparison of data to theory is still underway.

## RESEARCH EFFORTS IN THE FIELD AT LARGE

The promising results seen over the last five years in Nb<sub>3</sub>Sn single-cell cavities has spurred on a new interest in coating multi-cells for the purpose of actual beam acceleration. Jefferson Laboratory in Newport News has recently upgraded their coating furnace to be able to coat CEBAF 5-cell cavities with end-groups [18, 19], with the intent of placing a Nb<sub>3</sub>Sn CEBAF cavity in a cryomodule for beam testing. At Fermi National Laboratory in Batavia, a large coating furnace capable of coating 9-cell ILC cavities or 650 MHz 5-cell PIP-II cavities is being put through its final commissioning runs, and the coating of a 9-cell is expected soon [20]. At CERN, work has begun on producing Nb<sub>3</sub>Sn on a copper substrate [21] – potentially far cheaper than the niobium substrate required by the vapour diffusion process. Methods such as chemical vapour deposition (CVD) are also being considered for the manufacturing of Nb<sub>3</sub>Sn cavities.

Although the performance of Nb<sub>3</sub>Sn now warrants the fabrication of multi-cell cavities for building prototype cryomodules, much work remains to push the performance of Nb<sub>3</sub>Sn to the limits suggested by theory. Success in this endeavour relies on a deep understanding of the current performance limitations and the nature of the material itself. Such remains the focus of the Nb<sub>3</sub>Sn programme at Cornell, which is primarily funded by the U.S. Department of Energy. The research efforts at Cornell have recently benefited from close access to the tools and experts from a wide range of non-accelerator backgrounds available as part of the new NSF Center for Bright Beams. This recent access to input from fields such as materials science, chemistry, and theoretical physics has made significant contributions to the understanding of Nb<sub>3</sub>Sn [11]. These have included simulations of the layer growth using joint density functional theory, imaging of the cross-section of the layer using state-of-the-art instruments such as the new electron microscopy pixel array detector (EMPAD), and theoretical estimates of flux entry fields and losses from trapped flux.

## CONCLUSION

Nb<sub>3</sub>Sn cavities coated at Cornell University have achieved usable gradients while out-performing the best niobium cavities at 4.2 K, demonstrating that this material is capable of delivering on its promise as a next-generation high efficiency material. The  $Q$ -slope seen in previous cavities has been shown to be suppressed by ensuring a successful handover

from the nucleation to the coating process resulting in a uniform coating devoid of thin film regions. Further improvements in performance can be achieved by minimising the amount of trapped flux by ensuring that thermal gradients and ambient magnetic field during the cooldown are minimised.

Although the performance shown here is already exciting in its own right, and the material is now ready to move to prototype cryomodules, there is plenty of room to improve before the limits assumed to be fundamental are reached.

## REFERENCES

- [1] D. L. Hall, J. J. Kaufman, M. Liepe, R. D. Porter, and J. Sears, "First Results From New Single-Cell Nb<sub>3</sub>Sn Cavities Coated at Cornell University," in *Proceedings of IPAC 2017*, Copenhagen, 2017. [Online]. Available: <https://doi.org/10.18429/JACoW-IPAC2017-MO0CA2>
- [2] D. L. Hall, M. Liepe, and J. Maniscalco, "RF Measurements on High Performance Nb<sub>3</sub>Sn Cavities," in *Proceedings of IPAC 2016*, Busan, May 2016. [Online]. Available: <https://doi.org/10.18429/JACoW-IPAC2016-WEPMR024>
- [3] S. Posen and D. L. Hall, "Nb<sub>3</sub>Sn superconducting radiofrequency cavities: fabrication, results, properties, and prospects," *Superconductor Science and Technology*, vol. 30, no. 3, p. 33004, 2017. [Online]. Available: <http://stacks.iop.org/0953-2048/30/i=3/a=033004>
- [4] E. Saur and J. Wurm, "Pr{ä}paration und Supraleitungseigenschaften von Niobdrahtproben mit Nb<sub>3</sub>Sn-Überzug," *Naturwissenschaften*, vol. 49, no. 6, pp. 127–128, Jan. 1962. [Online]. Available: <http://dx.doi.org/10.1007/BF00621122>
- [5] S. Posen, "Understanding and Overcoming Limitation Mechanisms in NB<sub>3</sub>SN Superconducting RF Cavities," Ph.D. dissertation, Cornell University, 2014.
- [6] S. Posen, O. Melnychuk, A. Romanenko, D. Sergatskov, Y. Trenikhina, D. L. Hall, and M. Liepe, "Cutout Study of a Nb<sub>3</sub>Sn Cavity," in *Proceedings of SRF 2015*, Whistler, Sep. 2015. [Online]. Available: <https://doi.org/10.18429/JACoW-SRF2015-TUPB049>
- [7] A. Godeke, "A review of the properties of Nb<sub>3</sub>Sn and their variation with A15 composition, morphology and strain state," *Superconductor Science and Technology*, vol. 19, no. 8, pp. R68—R80, Aug. 2006. [Online]. Available: <http://stacks.iop.org/0953-2048/19/i=8/a=R02?key=crossref.b011eb22ef1c1d3f8f2c161fc5a2d175>
- [8] T. A. Arias, M. C. Payne, and J. D. Joannopoulos, "Ab initio molecular dynamics: Analytically continued energy functionals and insights into iterative solutions," *Phys. Rev. Lett.*, vol. 69, no. 7, pp. 1077–1080, Aug. 1992. [Online]. Available: <https://link.aps.org/doi/10.1103/PhysRevLett.69.1077>
- [9] S. Ismail-Beigi and T. A. Arias, "New algebraic formulation of density functional calculation," *Computer Physics Communications*, vol. 128, no. 1, pp. 1–45, 2000. [Online]. Available: <http://www.sciencedirect.com/science/article/pii/S0010465500000722>
- [10] R. Sundararaman, D. Gunceler, K. Letchworth-Weaver, K. Schwarz, and T. A. Arias, "JDFTx (<http://jdftx.org/>),"

2012. [Online]. Available: <https://jdf.tx.sourceforge.net>
- [11] D. L. Hall, J. J. Kaufman, M. Liepe, and J. Maniscalco, "Surface Analysis Studies of Nb<sub>3</sub>Sn Thin Films," in *Proceedings of IPAC 2016*, Busan, May 2016. [Online]. Available: <http://dx.doi.org/10.18429/JACoW-IPAC2016-WEPMR023>
- [12] J. Ding, D. L. Hall, and M. Liepe, "Simulations of RF Field-induced Thermal Feedback in Niobium and Nb<sub>3</sub>Sn Cavities," Lanzhou, 2017, presented at SRF2017, Lanzhou, China, paper THPB079, this conference.
- [13] M. Peiniger, M. Hein, N. Klein, G. Mueller, H. Piel, and P. Thuenus, "Work on Nb<sub>3</sub>Sn cavities at Wuppertal," in *Proceedings of The Third Workshop on RF Superconductivity*, Lemont, Illinois, Sep. 1988.
- [14] D. L. Hall, M. Liepe, R. D. Porter, D. B. Liarte, and J. P. Sethna, "Field-dependence of the Sensitivity to Trapped Flux in Nb<sub>3</sub>Sn," Lanzhou, 2017, presented at SRF2017, Lanzhou, China, paper THPB042, this conference.
- [15] S. Posen, N. Valles, and M. Liepe, "Radio Frequency Magnetic Field Limits of Nb and Nb<sub>3</sub>Sn," *Phys. Rev. Lett.*, vol. 115, no. 4, p. 47001, Jul. 2015. [Online]. Available: <https://link.aps.org/doi/10.1103/PhysRevLett.115.047001>
- [16] D. L. Hall, M. Liepe, R. D. Porter, P. Cueva, D. B. Liarte, D. A. Muller, and J. P. Sethna, "Cavity Quench Studies in Nb<sub>3</sub>Sn Using Temperature Mapping and Surface Analysis of Cavity Cut-outs," Lanzhou, 2017, presented at SRF2017, Lanzhou, China, paper THPB041, this conference.
- [17] A. Sheikhzada and A. Gurveich, "Dynamic transition of vortices into phase slips and generation of vortex-antivortex pairs in thin film Josephson junctions under dc and ac currents," *Physics Review B*, vol. 95, 2017.
- [18] G. Eremeev, K. Macha, C. Reece, A.-M. Valente-Feliciano, and U. Pudasaini, "Commissioning of Nb<sub>3</sub>Sn Multicell Cavity Coating System at JLab," Lanzhou, 2017, presented at SRF2017, Lanzhou, China, paper TUPB105, this conference.
- [19] C. Reece, G. Eremeev, U. Pudasaini, J. Tuggle, and M. Kelley, "Nb<sub>3</sub>Sn Developments at JLab," in *Presented at the Tesla Technology Collaboration meeting at Michigan State*, Lansing, 2017.
- [20] S. Posen, M. Merio, A. Romanenko, and Y. Trenikhina, "Fermilab Nb<sub>3</sub>Sn R&D Program," in *Proceedings of SRF 2015*, Whistler, 2015. [Online]. Available: <https://doi.org/10.18429/JACoW-SRF2015-TUPB048>
- [21] G. J. Rosaz, S. Aull, K. Ilyina, A. Sublet, and W. V. Delsolaro, "SRF Cavity Coatings: Review of Alternative Materials and Coating Techniques," Lanzhou, 2017, presented at SRF2017, Lanzhou, China, paper WEXA04, this conference.